Journal of Electroceramics 5:2, 111–125, 2000

Ionic Conductor Composites: Theory and Materials

P. KNAUTH

Laboratoire de Physico-Chimie des Matériaux, Université de Provence, Centre de St Charles, Case 26, F-13331 Marseille Cedex 3, France

Submitted October 14, 1999; Revised November 18, 1999; Accepted November 18, 1999

Abstract. The main theoretical concepts on ionic conduction at interfaces, especially the space charge layer model, are summarized in the first part of this review: ion trapping or redistribution leads to charge carrier accumulation, depletion or inversion and, consequently, to conductivity changes in composite materials. Experimental confirmations of the space charge layer model and the complementary percolation model are discussed. Major developments of ionic conductor composite materials over the last 25 years are presented in the second part, including lithium and other alkaline ion conductors, copper and silver ion conductors, di- and trivalent cation and anion conductors, glass and polymer composites. Some future trends and research needs are indicated in conclusion.

Keywords: solid state ionics, interfaces, space charge model, percolation

1. Introduction

Composite materials are heterogeneous mixtures of solid phases. The elaboration of composites offers a new degree of freedom in the search for advanced functional materials, because specific properties can to a certain degree be tailored by mixing appropriate phases. In the domain of solid state ionics, two routes can lead to improved solid ionic conductors: a search for new compounds and structures sustaining high levels of ionic conductivity or a modification of existing compounds, by heterogeneous or homogeneous doping. The latter involves homogenous dissolution of a certain amount of aliovalent dopant in the bulk of the ionic conductor M^+X^- in order to increase the concentration of mobile charge carriers according to bulk defect equilibrium. One example is the creation of additional metal vacancies by doping with cations of higher valence, such as D^{2+} in substitution of M^+, written in Kröger-Vink nomenclature [1]:

$$DX_2 + 2M_M \rightarrow D_M^{\bullet} + V_M' + 2MX \qquad (1)$$

Heterogeneous doping, in contrary, involves mixing with a second phase with very limited solid solubility and the formation of defect concentration profiles in the proximity of interfaces. The deviations from local electrical neutrality (space charges) are a consequence of point defect equilibrium at interfaces [2]. Apart the improvement of the electrical properties, such as high conductivity and ionic transference number, the development of composite materials can also lead to better mechanical properties, such as better shock resistance or higher strength. Although composite materials can in principle contain many different phases, literature in the field of solid state ionics deals primarily with two-phase mixtures.

In 1973, Liang [3] observed an enhancement of ionic conductivity by a factor of almost 50 in a composite material made from lithium iodide LiI, a compound with moderate Li^+ ion conductivity at ambient temperature, and dispersed small alumina Al_2O_3 particles. The maximum lay around 40 vol % alumina. After this initial study, the conductivity enhancement in heterogeneous materials was confirmed for numerous ceramic composites, including dispersions of fine insulator particles in an ionic conductor matrix and mixtures of two different ionic conductors, with a major contribution by J. B. Wagner [4] and his group. The majority of studies was made on monovalent cation conductors, such as lithium,

silver and copper halides, the largest group being lithium compounds, given their importance in high energy density portable batteries. Besides Al_2O_3, other oxides, such as MgO, SiO_2, CeO_2, TiO_2 and ferroelectric $BaTiO_3$, were found to be effective second phases for ionic conductivity improvements. More recently, the composite effect was also observed in ceramic anion conductors, such as lead or calcium fluoride, and even in inorganic solids with trivalent cation conductivity, like aluminium and rare-earth wolframates.

The theory of ionic conductor composites, which is developed in the first part, highlights the importance of phase boundaries for the electrical properties. Boundaries can be transport pathways or transport barriers, given their modified core structure (core effects), and can affect the charge carrier distribution in the adjacent regions (space charge effects). Local deviations from electrical neutrality in the vicinity of interfaces were recognized long time ago in the electrochemistry of liquid electrolytes or in colloidal systems. Gouy [5] established the theory of the electrical double layer at the electrode-electrolyte interface already in 1903 and Overbeek and co-workers [6] the electrostatic colloid theory in 1948. Lehovec [7] calculated in 1953 the defect distribution at the surface of ionic crystals and discussed the implications for ionic conduction. In 1972, Wagner [8] used the space charge layer concept to explain conductivity effects in two-phase materials with electronic conduction, such as metallic inclusions in a semiconducting oxide or mixtures of two semiconducting oxides. After an attempt by Jow and Wagner in 1979 [9], Maier [2,10,11] established the space charge layer theory of heterogeneous ionic conductors after 1984.

In the second part, we present important investigations of ionic conductor composites since Liang's initial study 25 years ago. Ceramic composites, which are mixtures of two crystalline inorganic phases, represent so far the most important group in solid state ionics, but a growing amount of work was recently devoted to glass-ceramic composites, obtained by partial crystallization of a glassy matrix, and polymer-ceramic composites, where an inorganic compound is dispersed in a polymer matrix. Agrawal and Gupta [12] recently reviewed composite solid electrolytes and gave an extensive list of systems reported in the literature.

2. Theory of Ionic Conduction in Composites

Interfaces play an important role for the transport properties of polycrystalline and polyphase (composite) materials. Given the anisotropy of boundaries, one has to distinguish between transport along and across interfaces. Enhanced ionic conduction along interfaces can be observed for two reasons.

First, the interface core itself is a disordered region, where defect formation and migration energies are generally notably reduced. This leads to enhanced ionic transport within the interface core (grain boundary diffusion). However, core effects are generally small, given the reduced interface area in conventional microcrystalline materials ($\sim d/L$, where boundary core width $d \approx 0.5$ nm and grain size $L \approx 1\ \mu$m). Some studies established the role of grain boundary diffusion in polycrystalline oxides, including NiO, Al_2O_3, MgO [13] or ZnO [14], but there seems to be no similar study in composite materials.

Second, point defect and dopant interactions with interfaces, for example accumulation in the interface core (intrinsic and extrinsic interfacial segregation), induce concentration profiles of point defects in the regions adjacent to the interface in ionic materials (space charge layers). Only few quantitative studies exist on grain boundary segregation in oxides, including CaO-doped ZrO_2 [15], TiO_2 [16] and CeO_2 [17], and similar studies on phase boundaries in composite materials are even more difficult, from an experimental as well as a theoretical point of view. The concentration profiles of mobile charge carriers near interfaces are a consequence of thermodynamic defect equilibrium, as we will see now.

2.1. Space Charge Layer Model

The fundamental concept is that ions can be trapped at the interface core. (This process is equivalent to a segregation phenomenon.) The counter species, in general a trapped ion vacancy, is then accumulated in the adjacent space charge regions. Driving force is the chemical affinity of a second phase to the trapped ion. For example, ''basic'' oxides present many nucleophilic hydroxide surface groups, which can attract and fix cations.

The space charge layer concept is a natural extension of volume defect thermodynamics, which takes the defect equilibrium at grain or phase

boundaries into account [2,10,11]. Assuming an ionic solid M^+X^- with Frenkel disorder, the bulk defect equilibrium:

$$M_M + V_i \rightarrow M_i^{\bullet} + V_M' \tag{2}$$

is established between metal interstitials $M_i^{\bullet}$ and metal vacancies V_M'. The Frenkel equilibrium constant reads:

$$K_F = [M_i^{\bullet}][V_M'] = \exp(-\Delta_F G^{\circ}/kT) \tag{3}$$

where the square brackets represent small defect concentrations and $\Delta_F G^{\circ}$ is the standard Gibbs free energy of formation of Frenkel defects.

The trapping of metal ions at interface sites can be written:

$$M_M + V_S \rightarrow M_S^{\bullet} + V_M' \tag{4}$$

Here, V_S and $M_S^{\bullet}$ are respectively an empty interface site and a metal ion trapped at an interface site. Supplementary metal vacancies are created in the adjacent space charge regions and, if the defect equilibrium is established locally, the number of interstitials is reduced because of the coupling Frenkel constant (Fig. 1).

At equilibrium, the electrochemical potential of charged species, such as metal vacancies, is constant across an interface, but the chemical potential changes. For a diluted system, the local electrochemical potential $\eta(x)$ can be written:

$$\eta(x) = \mu(x) + z_i F \phi(x) \tag{5}$$

where $\phi(x)$ is the local electrical potential, z_i the defect charge and F Faraday's constant. The local chemical

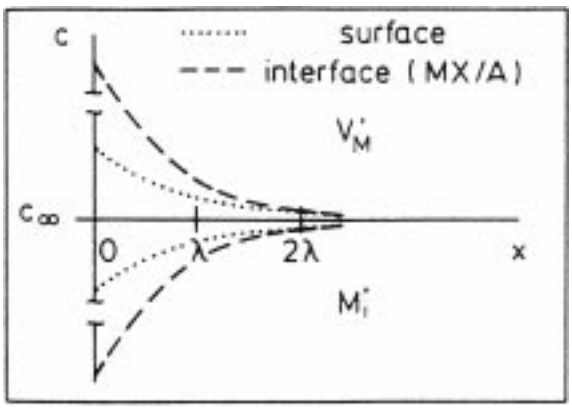

Fig. 1. Defect concentration profiles near a phase boundary (with gas phase or insulating oxide A) [2].

potential $\mu(x)$ is related to the molar concentration of defect $[i]$ (R is the universal gas constant).

$$\mu(x) = \mu^{\circ} + RT \ln[i](x) \tag{6}$$

The standard term μ° contains concentration independent entropy and energy parameters. The equilibrium condition is:

$$d\eta(x) = 0 = d(RT \ln[i](x) + z_i F \phi(x)) \tag{7}$$

so that the monotonous defect concentration profile in the space charge region can be expressed as:

$$[i](x)/[i]_{\infty} = \exp[-z_i F(\phi(x) - \phi_{\infty})/RT] \tag{8}$$

The bulk concentration $[i]_{\infty}$ is a function of temperature, chemical potential and doping. The local concentration in the space charge region $[i](x)$ depends on the difference between the bulk and the local electrical potential, ϕ_{∞} and $\phi(x)$. For $\phi(x) > \phi_{\infty}$, the concentrations of all negative defects are raised by the exponential factor, while those of the positive defects are reduced by the same factor and vice versa for $\phi(x) < \phi_{\infty}$.

The variation of defect profiles is observed over a distance approximately twice the Debye length λ, that is conveniently defined, like in semiconductor and liquid electrolyte theory, with respect to the bulk defect concentration $[i]_{\infty}$ ($\varepsilon\varepsilon_0$ is the dielectric permittivity) [10]:

$$\lambda^2 = \varepsilon\varepsilon_0 RT/(2z_i^2 F^2 [i]_{\infty}) \tag{9}$$

Space charge effects are pronounced at reduced temperature, due to the low bulk defect concentrations. If the majority charge carriers are accumulated in the space charge regions, a considerable conductivity enhancement may result; given that a vacancy mechanism is observed in most solid ionic conductors at reduced temperature (extrinsic domain), ion trapping can lead to a major enhancement of the ionic conductivity.

2.2. *Conductivity Equations*

The conductivity contribution of a single interface (bicrystal experiment) can be calculated analytically by integration of the conductivity profile from the interface to the bulk [10]. The calculation of the conductivity of a two-phase mixture, for example an ionic conductor/insulator composite, requires simplifications of the distribution topology, because there

exists a complex superposition of various transport paths by bulk and interfaces.

Ionic conductor/insulator composites. Maier [2,10, 11] assumed a three-dimensional network of percolating paths with simple cubic symmetry. All components perpendicular to the current direction cancel out, while the remaining components with mean specific conductivity σ_i are connected in parallel and can be combined to an ''effective'' volume fraction $\beta_i\varphi_i$, which contributes to the quasi-parallel circuit. The correction factor β_i takes values between 0.2 and 0.7. Neglecting transfer resistances, it follows that the conductivity of the composite can be written:

$$\sigma = \sum \beta_i \varphi_i \sigma_i \tag{10}$$

The physical reason for the formation of continuous conduction paths is the nature of the interfacial interactions. In the case of composites with dispersed insulator particles, the small size of the insulator particles with respect to the ionic conductor grains contributes to formation of continuous particle monolayers, resembling the wetting of grains by a liquid phase.

For a large enhancement, the conductivity of the space charge region is a function of the geometric mean of the carrier concentration in the bulk $[i]_\infty$ and in the first layer adjacent to the interface $[i]_0$:

$$\sigma_{sc} = z_i F \mu_i ([i]_0 [i]_\infty)^{1/2} \tag{11}$$

For cubic grains, the effective volume fraction of space charge regions can be written as:

$$\varphi_{(sc)} = \beta(3\varphi_A / r_A) 2\lambda \tag{12}$$

where φ_A is the volume fraction of second phase with mean grain size r_A. If the contributions of the insulator phase and the interface core (boundary diffusion) are neglected and the definition of the Debye length, Eq. (9), is used, the conductivity of the composite can be written:

$$\sigma = (1 - \varphi_A)\sigma_\infty + \beta(3\varphi_A / r_A)(2\varepsilon\varepsilon_0 RT[i]_0)^{1/2}\mu_i \tag{13}$$

The first term describes the bulk conductivity and takes into account that the ionic conductor is partly replaced by insulator in the composite.

Mixtures of ionic conductors. Conductivity anomalies in a miscibility gap were detected in mixtures of two solid ionic conductors with Frenkel disorder, such as AgBr-AgI [18] and AgCl-AgI [19,20]. Here, a silver ion can not only pass from one ionic conductor AgX to the interface, but also into the space charge layer of the neighboring ionic conductor AgX':

$$Ag_{Ag}(AgX) + V_i(AgX') \rightarrow Ag_i^{\bullet}(AgX') + V'_{Ag}(AgX) \tag{14}$$

In this way, the vacancy concentration is enhanced in one ionic conductor and the interstitial concentration in the other. Equivalently, this process can be described by a transfer of $Ag_i^{\bullet}$ or V'_{Ag} between the two ionic conductors. The situation is analogous to the contact potential formed between two electronic conductors. The redistribution of mobile ions is due to a difference of standard Gibbs free energies of defect formation. Figure 2 illustrates the processes during establishment of contact equilibrium, concentration profiles and measured conductivities in the system AgBr-AgI [2,18]. At the contact between two ionic conductors with Schottky disorder, such as LiBr-LiI [21], large effects are not expected in absence of charge accumulation at the phase boundary [2].

Nanocomposites. The trapping effects can be particularly important in nanocrystalline materials, which present a very large interface density. If the grain size L of the ionic conductor, or more generally the distance between interfaces or extended defects, becomes comparable with the Debye length, the space charge regions overlap and the grains are charged throughout, as illustrated in Fig. 3 [22,23]. In nanoceramics, the thermodynamic bulk defect concentrations are not reached and the thermodynamic standard potential becomes size-dependent. This is similar to the quantum size effect in solid state electronics. An additional increase of conductivity can be expected in the accumulation case and described by a ''nano-size'' factor [24]:

$$g = (4\lambda / L)[([i]_0 - [i]^*)/[i]_0]^{1/2} \tag{15}$$

$[i]^*$ is the defect concentration in the grain center. For a large effect, $g = (4\lambda/L)$, and a grain size $L = 0.4\lambda$, the conductivity would be enhanced by a supplementary order of magnitude.

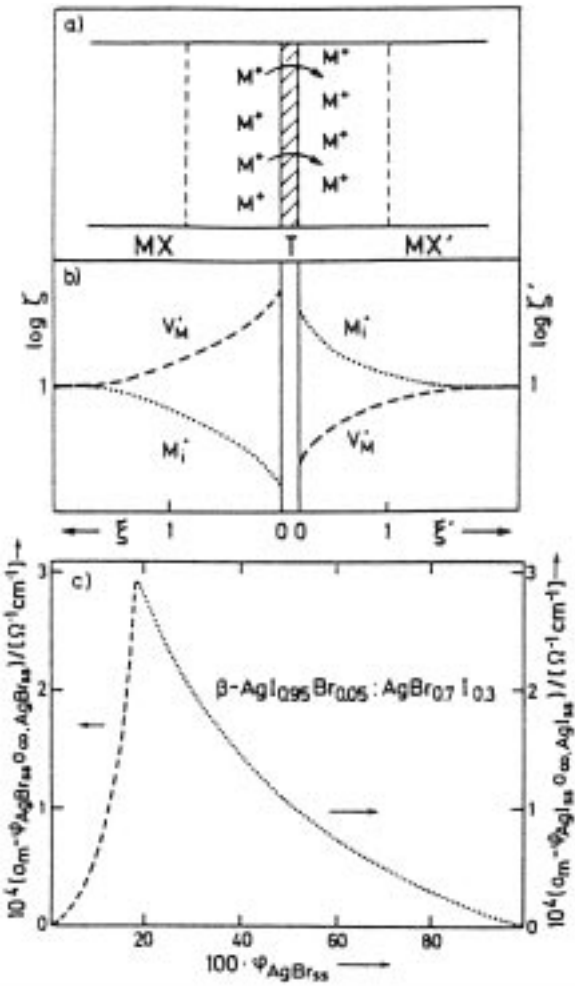

Fig. 2. (a) Contact equilibrium between two ionic conductors with Frenkel disorder, (b) defect concentration profiles, (c) experimental conductivity data [2].

2.3. Experimental Verifications of the Space Charge Layer Concept

The space charge layer model takes an idealized view of the interface. A major assumption is that the bulk structure is maintained up to the atomic layer in contact with the interface core: the variation of the materials parameters is assumed to take the form of a step function (abrupt core-space charge layer model). A continuous property variation due to a structural adjustment and energy gradients is more realistic in some cases, but is also more difficult to implement in a quantitative model. Several other processes can lead to a change of ionic conductivity.

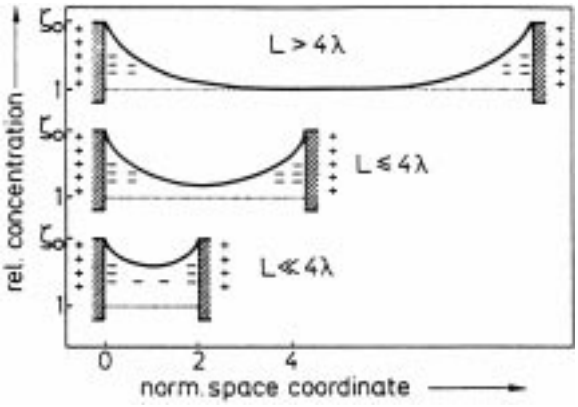

Fig. 3. Defect concentration profiles in a nanostructured composite for different grain sizes L [2].

1. Impurities may diffuse from the interface and create mobile defects or act themselves as charge carrier, e.g., protons. However, the latter process should modify the activation enthalpy. Major impurity effects were ruled out at least in the case of AgCl-alumina composites [25], but a small contribution is possible.
2. Extended defects, such as dislocations, can be formed to compensate the lattice misfit. Furthermore, transient defects can be formed during composite processing, e.g., due to different thermal expansion coefficients after a heat treatment. However, non-stationary dislocations can normally be healed out by an annealing treatment. Stress and dislocation effects on the conductivity were studied for AgCl composites [26] and for LiI thin films deposited on a ceramic substrate [27]. Phipps and Whitmore discussed a new pathway with changed activation enthalpy in LiI-SiO_2 composites [28].
3. An ordered ''two-dimensional'' compound can be formed as a consequence of thermodynamic interface equilibrium and metastable phases can also be observed. Jiang and Wagner [29] presented a model, in which the conductivity increase of composites was attributed to the formation of an amorphous phase at the interface. The very large conductivity enhancement in AgI-Al_2O_3 composites could be explained by the existence of layered AgI polytypes [30].

In essence, most of the described phenomena provide a new conduction mechanism in the zone adjacent to the boundary and therefore an activation

enthalpy unlike the bulk value. Experimentally, most composite materials show however an activation enthalpy comparable to the bulk defect migration enthalpy. In the space charge layer model, changes of the defect chemistry of the material are considered to introduce only small perturbations of defect mobility and defect thermodynamic data. In the low temperature regime, the temperature dependence of conductivity is due to the thermal activation of ion hopping. For large effects, defect formation and association are often negligible and the model predicts that the activation enthalpy is equal to the migration enthalpy of the accumulated defect. The good agreement of composite activation enthalpies with bulk migration enthalpies shows that this assumption is not in contradiction with the reality. Taking a small temperature dependence of the defect concentration into account, the Arrhenius-type dependence of conductivity of AgCl and AgBr composites with alumina could be quantitatively interpreted by Eq. (13) in an intermediate range of Al_2O_3 concentrations [10].

Many other experimental observations are in agreement with the space charge layer model. The assumed quasi-parallel switching, Eq. (10), is in accordance with impedance spectra of AgCl-Al_2O_3 composite materials [11]. The high frequency arc is determined by the high conductivity interfacial paths short-circuiting the bulk and the dielectric constant of the bulk, whereas the low-frequency branch reveals minor blocking effects, due to alumina particles which narrow the current paths.

TlCl-Al_2O_3 composites are an interesting example, where a charge carrier inversion layer is observed [31]. Pure TlCl is an anion conductor with Schottky disorder, but Tl^+ ions are fixed at phase boundaries with nucleophilic alumina, so that thallium vacancies are enriched in the space charge regions. When sufficient alumina is added, cation conduction becomes predominant, evidenced by a change of activation enthalpy. Here, a charge carrier inversion and a $V_{Cl}^{\bullet}$–V'_{Na} junction between ionic charge carriers are observed, analogous to a *p*–*n* junction in a semiconductor.

The suggested atomic mechanism for conductivity enhancement in the case of cation conductor composites with second phase oxide particles is the fixation of cations on hydroxide surface groups. This interpretation is confirmed by experiments with surface-modified oxides [32], including alumina particles treated with chlorotrimethylsilane, where the reaction:

$$\text{-OH} + (CH_3)_3\text{-SiCl} \rightarrow \text{HCl} + \text{-OSi}(CH_3)_3 \quad (16)$$

reduces the number of hydroxide surface groups. The smaller conductivity enhancement found for AgCl composites with this surface-modified Al_2O_3 was recently confirmed for AgI-Al_2O_3 composites using a similar treatment. XPS analysis is consistent with a substitution of hydroxide by silane groups on the alumina surface [33]. In this context, the order of oxide activity ($Al_2O_3 > SiO_2$) in composites corresponds to the pH values of zero charge ($pH(Al_2O_3) = 9$, $pH(SiO_2) = 4$) [2]. Experiments with AgCl melts confirmed the complete wetting of basic oxide surfaces, such as γ-Al_2O_3 and MgO [2].

Apart conductivity effects, the use of composite solid electrolytes seems very promising for heterogeneous catalysis, given that the increased defect concentrations near interfaces in composites can significantly enhance the rate of chemical or electrochemical reactions. Simkovich and Wagner [34] reported an increase of the rate of the HCl elimination reaction:

$$(CH_3)_3CCl \rightarrow HCl + (CH_3)_2C = CH_2 \quad (17)$$

in presence of $CdCl_2$-doped AgCl, due to the increased bulk concentration of silver vacancies (homogeneous doping). Similar experiments [35] with AgCl-Al_2O_3 composites showed a very large rate enhancement, e.g., at 150°C no significant reaction was observed with pure AgCl, whereas the equilibrium was reached after 20 min with the composite material. The effect of pure Al_2O_3 was much lower. The proportionality of the effective rate constant to the number of composite pellets (active area) suggested that surface adsorption was the rate-limiting process. An evaluation of the mass action constant gave a unique line, as expected for a catalytic effect. Aoyama et al. [36] showed that AgCl-Al_2O_3 catalysts are highly active for the NO conversion with ethanol as reductant even in the presence of SO_2. The catalysts were prepared by impregnation of nano-size alumina powders with aqueous solutions of silver nitrate and ammonium chloride. The high activity was ascribed to the important dispersion of crystalline AgCl particles on the supporting Al_2O_3, but was not discussed from a defect chemical point of view.

Recently, Vennekamp and Janek [37] presented the theory of ionic thermopower for the case of composite solid electrolytes. Ionic thermopower is determined by the point defect equilibrium, such as the cation Frenkel equilibrium in AgCl. However, the different local distributions of defects created either by homogeneous doping or in space charge layers near interfaces can not be detected by thermo-emf measurements.

2.4. Percolation Model

Although the analytical Eq. (13) is in good agreement with the experiment for many composite systems in an intermediate range of composition, a linear relation can not describe the behavior near critical points. Two thresholds can be discussed in ionic conductor/insulator composites. For a small concentration of second phase, the space charge regions are isolated in the matrix of ionic conductor and do not effectively contribute to ionic conductivity enhancement. There exists a first critical concentration, where a continuous network of highly conducting paths, extending through the whole sample, appears. With further increase of second phase concentration, the conductivity increases drastically: this is the domain where a linear relation may apply. At large volume fractions of insulator material, we arrive at a second critical concentration, where conduction paths become disrupted, because continuous layers of insulator grains are formed (conductor-insulator transition). The conductivity drops sharply after this second threshold (Fig. 4).

Effective medium theories [38–42] are unable to describe the behavior near critical points, because property fluctuations are here important. Critical phenomena can however be described in the framework of percolation theory, first applied to the problem of ionic conductor/insulator composites by Bunde et al. [43–44], Bunde [45] and Roman and Yussouf [46]. One should mention here that Van Siclen [47] applied very recently a walker diffusion method to calculate the conductivity of disordered two-phase composites, where the walker density is proportional to the conductivity of the phases. The initial model of Bunde et al. made a certain number of assumptions, which do not correspond to the experimental evidence. First, equal grain sizes of ionic conductor and insulator were assumed, although in most experiments, microcrystalline ionic conductor

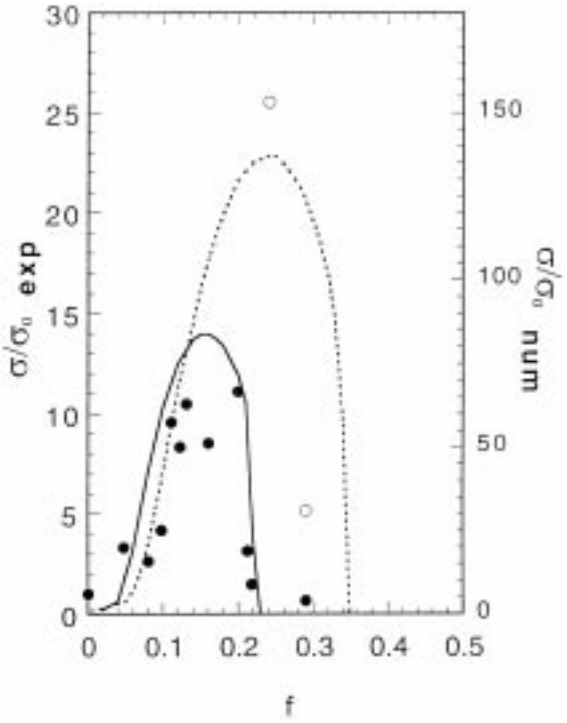

Fig. 4. Percolation thresholds in CuBr-TiO_2 composites [98]. σ/σ_0 is the normalized conductivity and f is the volume fraction of TiO_2. The dots are experimental data and the curves are numerical simulations. Reducing the mean grain size of the ionic conductor from 5 μm (black dots) to 3 μm (open dots) leads to a larger conductivity enhancement.

grains and nanocrystalline insulator grains were used. Roman et al. [46] later simulated the effect of a variation of the insulator grain size in a two-dimensional system. Second, a random distribution of ionic conductor and insulator particles was assumed, but in the experiments, the interfacial interactions and the small size of insulator particles lead to the formation of continuous layers of insulator around the large grains of ionic conductor.

Both experimental facts were taken into account in the improved percolative transport model by Debierre et al. [48]. A bell-shaped curve of conductivity versus volume fraction of insulator was simulated when the ionic conductor grain size was assumed constant, which is the case in systems with moderate interfacial interactions. A linear relation was obtained, when the variation of the ionic conductor size L with the volume fraction of insulator $\varphi_A (L \propto 1/\varphi_A)$ was taken into account [49]. Furthermore, very high conductivities were calculated for very small grain sizes of both

components (nanocomposites) [48]. Recent simulations with a bimodal size distribution of ionic conductor confirmed that the mean size approach is appropriate [50]. One should mention that a scaling approach was recently proposed to describe the dispersion behavior of brushite ($CaHPO_4$ 2 H_2O)-polymer composites, especially near the insulator/conductor percolation threshold [51]. The dielectric properties and impedance spectra of composites were first simulated by Blender and Dieterich using random ac networks [52]. The percolation models are complementary to the analytical approach; the physical model relies in both cases on the space charge layer concept.

3. Materials

Tables with the composition and properties of many ceramic, glass and polymer composites can be found in a recent article by Agrawal and Gupta [12]. We highlight in the following some of the most significant developments in the last 25 years, since Liang's discovery of enhanced ionic conductivity in a composite material.

3.1. Processing and Characterization

Preparation. Most of the ceramic composites were prepared by conventional milling of dry powders followed by compression, typically under some kbar. In many studies, the pellets were heated above the melting temperature of the ionic conductor, cooled and reground before the final pelletizing, to ensure a better mixing of the components. Dispersoid insulator particles in an ionic conductor matrix should be as small as possible, preferentially with submicron grain size, in order to reach a good contact between the two phases and to avoid blocking effects. To obtain reproducible results, it is very important to eliminate transient defects due to the preparation, such as dislocations, by an annealing treatment at moderate temperature.

However, more elaborate fabrication routes were also proposed. (1) Deposition of ionic conductor within micro-pores of a porous insulator matrix, particularly Al_2O_3 [53]: unlike conventional methods, the effects of substrate anisotropy, grain orientation etc. on ionic conductivity could be studied [54–56]. (2) Thermal decomposition of appropriate precursor materials: Rog et al. [57] mixed CaF_2 and the aluminium salt of 8-hydroxyquinoline, which was decomposed during heating into fine Al_2O_3 particles dispersed in the CaF_2 matrix. Köhler et al. [58] described the preparation of $Al_2(WO_4)_3 - Al_2O_3$ composites by controlled thermal decomposition of $Al_2(WO_4)_{3-x}(MoO_4)_x$ solid solutions. Volatile MoO_3 was evaporated from the sample under nitrogen flow and a composite with size distribution of alumina particles was obtained. 3) Precipitation from aqueous solutions containing insoluble oxide particles, e.g., CaF_2 and PbF_2 from $Ca(NO_3)_2$ and $Pb(NO_3)_2$ solutions with Al_2O_3 particles by adding NH_4F [59,60], or drying solutions containing ceramic precursors, such as Li_2SO_4 and $Al(OH)_3$ [61] or CsCl and Al_2O_3 particles [62] (solution casting method). (4) Partial crystallization of glassy materials to prepare glass-ceramic composites [63,64]: here, the ceramic particles often present sizes in the nanometer range.

Characterization. X-ray diffraction was the most employed structural characterization technique, because it informs on formation of intermediate compounds and extended solid solubility between the components and also, more or less reliably, on the mean grain sizes of the two phases. Scanning electron microscopy was used to observe the sample morphology. However, the microstructure at the atomic level is not easy to observe (for example by transmission electron microscopy TEM), given the difficulties in sample preparation for TEM, because in most thinning techniques, like ionic milling, one phase (often the ionic conductor) is preferentially etched away.

Impedance spectroscopy is by far the most important electrical characterization technique, because it permits to separate the contributions of bulk and blocking grain boundaries. An ionic depletion layer was detected by Maier and coworkers at the interface between a single crystal of AgCl (or AgBr) and electronically conducting oxides, such as RuO_2 or $La_{0.5}Sr_{0.5}CoO_3$, under blocking conditions [65] and for a composite with multiple interfaces of random orientation. Electronic conductivities were measured using the Hebb-Wagner dc polarization technique [2].

Ionic mobilities in composites were studied by NMR spectroscopy, notably with Li ion conductors, given that high resolution ^{7}Li NMR is available [66]. Lunden et al. [67] studied self-diffusion in composites

using a mass spectrometric technique and radioactive tracers.

Thermoanalytical techniques, such as differential thermal analysis, and calorimetry were applied to check the absence of significant amounts of new phases or modifications of phase transition temperatures, notably in the case of AgI composites [68–70].

3.2. *Lithium Ion Conductors*

After Liang's discovery of the enhanced ionic conductivity in LiI-Al_2O_3 composites (Fig. 5 [3]), Pack et al. [71] showed the importance of water in undried samples. Even higher increases, by two to three orders of magnitude, were found later by Poulsen et al. [72] for a large number of LiI-Al_2O_3 compositions, independently of the source of the starting materials and the fabrication route. High resolution ^{7}Li NMR demonstrated the presence of at least two distinct Li^+ sites; their proportion depended on temperature and composition. At 50 vol % alumina, the population of bulk Li ions was almost identical to that in the interface regions. This result is in agreement with the experimentally observed reduction of the ionic conductor grain size with increasing alumina concentration and reflects the very large effective interfacial regions in this material [66]. The composite LiI-Al_2O_3 was one of the few solid electrolytes put into practical use in commercial batteries: $Li/LiI\text{-}Al_2O_3/PbI_2/Pb$ [3] and $Li/LiI\text{-}Al_2O_3/TiS_2/S$ [73]. In the ionic conductor analogue of semiconductor sensors, surface conductivity variations upon adsorption of gases are a result of chemical interactions of acid-base type. The transfer resistance, which plays a decisive role for response time and selectivity of electrochemical sensors at reduced temperature, is largely controlled by defect concentrations at the interface, so that heterogeneities, for example in a composite material, can reduce the transfer resistance. A material composed of 10% LiF dispersed in γ-Al_2O_3 can be used as conductometric humidity sensor. The conductivity change was attributed to water adsorption at the LiF/Al_2O_3 boundary [74].

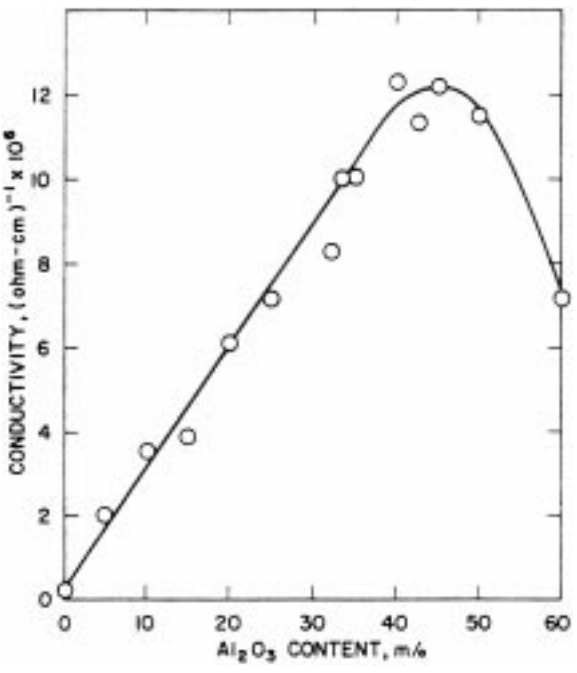

Fig. 5. Conductivity of LiI-Al_2O_3 composites as function of the alumina concentration [3].

The ionic conductivity enhancement of LiI films grown with strongly preferred orientation on sapphire substrates was not stable, but decreased during annealing at the growth temperature. The data were consistent with the presence of transient dislocations [27]. The film/substrate interfacial area was here too small to observe an important space charge effect. Phipps and Whitmore [28] reported an enthalpy of migration in LiI-SiO_2 mixtures that was only a third of the bulk value. This was attributed to LiI lattice distortion near the interface, another of the few examples, where a ''new'' conduction pathway was proposed.

Li_2SO_4 is not only a lithium-ion conductor, but also a proton conductor in hydrogen-containing atmospheres. Mellander et al. studied several composite materials containing Li_2SO_4. The ionic conductivity of Li_2SO_4-Al_2O_3 composites [75] increased with increasing Al_2O_3 content, up to a maximum at about 43 mol % Al_2O_3. However, XRD patterns suggested that intermediate phases were formed at this alumina concentration. The temperature of the β–α phase transition of Li_2SO_4 decreased with increasing Al_2O_3 concentration, so that the α-phase was stabilized to lower temperature by adding alumina. Zhu et al. designed hydrogen fuel cells with the mixed lithium- and proton-conducting Li_2SO_4-Al_2O_3 composite electrolyte [75]

An ionic conductivity enhancement was also reported for mixtures with other Li-ion conductors. In the Li_2SO_4-Li_2CO_3 system [76], the ionic

conductivity maximum lay close to the eutectic concentration, where the grain size had a minimum. Singh and Bhoga [77] obtained a glass-ceramic composite by adding a low-melting ionic conducting glass of approximate composition 6 Li_2O-4B_2O_3-ZrO_2 to fill the pores of the composite material with eutectic composition. In the Li_2SO_4-LiCl and Li_2SO_4-LiBr systems [67], cation and anion self diffusion was measured using a mass spectrometric technique. Cation and anion diffusion coefficients increased with increasing concentration of lithium halide. Composites Li_2SO_4-Ag_2SO_4 were used to design potentiometric SO_2 and SO_3 sensors, based on the cell: Ag/Li_2SO_4-$Ag_2SO_4/SO_2, SO_3, O_2$ [78]. The reference electrode was prepared by embedding silver powder into part of the two-phase electrolyte. The potential measured with the two-phase sulfate sensor was more stable and accurate than with pure silver sulfate.

Ternary lithium halides with the inverse spinel structure Li_2MX_4, are also Li^+ ion conductors. The effect of an addition of ceria particles on the conductivity of Li_2MnCl_4, was studied by Jacob et al. [79]. Nagai and Nishino [80] found nearly one order of magnitude increase of conductivity for Li_3PO_4-Al_2O_3 composites prepared by deposition into a porous alumina matrix.

3.3. Other Alkaline Ion Conductors

Guth et al. [81] and Brosda et al. [82] described composites of $K_2YZr(PO_4)_3$ and M_2SO_4(M = Na, K) with Al_2O_3 and also mixtures M_2CO_3-$BaCO_3$ and M_2SO_4-$BaSO_4$. In the last system, which presents a domain of solid solubility (dissolution of $BaSO_4$ up to 5 mol %), the conductivity enhancement could be interpreted by mixed homogeneous and heterogeneous doping. The maximum increase lay in the two-phase region. Apart the conductivity effect, K_2SO_4-$BaSO_4$ electrolyte membranes had a better gas tightness in potentiometric SO_2 sensors.

In materials with high dielectric constant, such as ferroelectrics near the Curie temperature, widely extended space charge regions and, hence, a high conductivity enhancement should be expected, cf. Eq. (13), but this prediction has apparently not been verified so far. A strong influence of the dielectric constant of tetragonal, ferroelectric $BaTiO_3$ particles as dispersed second phase on the conductivity of $Na_4Zr_2Si_3O_{11}$, one of the end members of the NASICON family, was reported [83,84] with a maximum in the vicinity of the ferroelectric phase transition. The frequency dependence of the ac conductivity indicated an increase of the Na^+ hopping rate rather than increased concentration [85]. The higher ion mobility, which was not observed in presence of cubic, paraelectric $BaTiO_3$, was attributed to surface dipole moments in the ferroelectric phase. However, the correlation with the dielectric constant could not be confirmed in a second study with lead-doped $BaTiO_3$ dispersoids [86].

Lavrova et al. [87] investigated the properties of composites of alkaline nitrates MNO_3 (M = Li, Na, K, Rb) with Al_2O_3 or SiO_2. In the case of $RbNO_3$ [88], different experimental techniques indicated the formation of an amorphous layer at the interface, responsible for the large conductivity increase. The possibility of proton conduction was not checked. The conductivity enhancement in CsCl-Al_2O_3 composites [62] could be interpreted in the framework of the space charge layer model. CsCl is a compound with Schottky-type disorder and the anion vacancies are more mobile than the cation vacancies, so that anion conduction is observed. However, the segregation of Cs^+ ions on the alumina surface leads to an increased cation vacancy concentration in the space charge regions, i.e., an inversion layer, and a change to cation conduction, evidenced by a slight increase of the activation enthalpy. Furthermore, the phase transition of CsCl was observed by DTA in the composites, but the conductivity curves were continuous at this temperature, indicating that the change of conductivity in the composite was due to interfacial conduction.

3.4. Copper and Silver Ion Conductors

Mesoscopic effects highlighting the importance of interfaces in composite materials are the stabilization of metastable phases and the variation of phase transition temperatures [89]. Interfacial interactions energies of the order of 0.5 eV in composite materials with alumina are great enough to cause phase transitions in a polymorphic compound, such as AgI. Furthermore, Coulomb interactions at high defect concentrations near interfaces can naturally lead to order-disorder phase transitions. AgI-Al_2O_3 composites showed the largest conductivity enhancement, by a factor 2000 for un-dried alumina [18,90]. The very large enhancement and a significant change of phase transition temperatures was confirmed by

Uvarov et al. [91]. This is outside the range of conventional space charge effects but can be explained by stacking fault formation at AgI-alumina phase boundaries [30]. New peaks in the XRD patterns could be attributed to a layered structure with stacking sequence ABCBCAC (7H-AgI), that can be separated into substructures exhibiting the sequence of hexagonal β-AgI and cubic γ-AgI. The stacking fault arrangement can be considered as an ionic heterostructure β-AgI/γ-AgI with a layer thickness below the Debye length, so that mesoscopic conductivity effects resulting from overlapping space charge regions, Eq. (15), are expected. The total AgI exists in the 7-layer polytype form if the alumina concentration exceeds 30 mol %.

Nagai and Nishino [53–56] published a series of papers on the preparation of AgI composites with up to ten times higher conductivity by precipitation of AgI, which showed a preferential orientation, into the micropores of an Al_2O_3 matrix. Composites AgCl-AgI-Al_2O_3 [92] were also prepared by this technique and showed a conductivity maximum at $\approx$ 25 mol % AgCl. A conductivity enhancement by one order of magnitude was also found in composites of [0.75 AgCl-0.25 AgI] with 10 mass % nano-size SiO_2 [93].

Recently, the properties of a composite between a Frenkel-disordered material AgCl and a Schottky disordered material NaCl were reported [94]: there is no reason for a significant conductivity increase from the point of view of defect chemistry in such composites, but the lamellar structure of the eutectics may be used as container for liquid electrolytes, such as $AgNO_3$ solutions, when the NaCl is selectively leached out with water. This is a possible strategy to combine the high conductivity of liquid electrolytes with the mechanical strength of a solid envelope.

During long time, copper ion conductor composites were much less studied than their silver analogues. However, composite materials of CuI with dye-sensitized TiO_2 show excellent properties for photovoltaic energy conversion in dye-sensitized solar cells (DSSC) [95]. Jow and Wagner [9] studied CuCl-Al_2O_3 composites, where a maximum conductivity enhancement by a factor of 20 was found. The dependencies on alumina grain size and volume fraction were described by a qualitative space charge layer model. Knauth and coworkers investigated CuBr composites with Al_2O_3 [96] or TiO_2 (anatase) [97,98]. The basicity of TiO_2 is lower than that of alumina, so that an imperfect wetting was observed with titania. The percolation behavior was simulated by a numerical model [48–50].

3.5. Di- and Trivalent Cation and Anion Conductors

Fujitsu et al. [99] reported a conductivity enhancement in composites of the Sr^{2+} ion conductor $SrCl_2$ with alumina and studied a multi-layered material composed of $SrCl_2$ films and Al_2O_3 thin plates. The measured conductivity of this sample, although higher than for pure $SrCl_2$, was smaller than the value calculated assuming ideal space charge layer formation, but the activation energy was in good agreement with bulk $SrCl_2$.

Recently, composites of trivalent cation conductors were reported. $Al_2(WO_4)_3$-Al_2O_3 composites were prepared by thermal decomposition of $Al_2(WO_4)_{3-x}(MoO_4)_x$ solid solutions [58]. A cation transference number of 97% and a four-fold conductivity increase were observed. These composites were used to measure and control the aluminum concentration in zinc hot-dip galvanizing baths [100]. A conductivity enhancement by a factor 2–4 was obtained for other rare-earth tungstate $M_2(WO_4)_3$–Al_2O_3 composites (M = Sc, $Sc_{0.8}Lu_{0.2}$) [101].

A conductivity enhancement was also found in composites of solid ionic conductors with anion Frenkel disorder, such as calcium or lead fluoride, and an insulator. The addition of 2.5 mol % dispersed Al_2O_3 to CaF_2 caused an ionic conductivity enhancement up to two orders of magnitude, depending on the preparation technique, but a conductivity decrease was observed for samples with more than 5% alumina [57]. A careful analysis of PbF_2 composites with dispersed SiO_2 and Al_2O_3 particles [59,60] revealed that the observed conductivity enhancement is due to an enhanced concentration of fluorine ion vacancy in the space charge layers, as consequence of interfacial adsorption of F^- ions :

$$F_F + V_A \rightarrow F'_A + V_{\dot{F}} \tag{18}$$

The larger conductivity enhancement with SiO_2 than with Al_2O_3 can be ascribed to the more acidic (anionophilic) character of SiO_2 compared to Al_2O_3. The even larger enhancements found with zirconia particles are a convincing further evidence for the adsorption model, because ZrO_2 is more acidic than SiO_2. One should mention here that Nagai et al. [102]

formed β-PbF_2 grains with preferred orientation inside porous alumina.

Feighery and Irvine [103] studied the effect of alumina additions upon the electrical properties of commercial yttria-stabilized zirconia. However, major space charge effects are not expected in this system, because the Debye length is small in ionic conductors with large homogeneous dopant concentration and oxygen ion adsorption on alumina surfaces is not very favorable. Small additions of alumina, below the solubility limit, caused a decrease of bulk conductivity and increase of grain boundary conductivity, possibly by reaction with silica impurities, segregated at the grain boundaries. The addition of alumina improved considerably the mechanical strength of the ceramics. Mori et al. used composites of stabilized zirconia with alumina as solid electrolytes in planar solid oxide fuel cells (SOFC) [104].

3.6. Glass and Polymer Composites

Glass and polymer composites are relatively new developments. Compared with the status reached with ceramic composites, the understanding of fundamental properties of these materials is much less developed. Glass ceramics, formed by crystalline inclusions inside a glassy matrix, are often nanocomposites, because the size of the crystallites is very small. Dispersed α-AgI microcrystals in AgI-based glass matrices of composition AgI-Ag_2O-M_xO_y ($M_xO_y = B_2O_3$, GeO_2, WO_3) were discovered by Tatsumisago et al. [63,105]. These glass ceramics exhibit high ionic conductivities and low activation energies at room temperature. The larger activation energies observed at lower temperatures were attributed to a positional ordering of Ag^+ ions in the microcrystals.

Adams et al. [64] showed that a pronounced increase of conductivity was observed during initial stages of devitrification of AgI-Ag_2O-M_xO_y glasses, when a crystalline phase with reduced Ag^+ conductivity was formed inside the glassy matrix. However, it was not clarified if an increase of carrier concentration or mobility near the interface is responsible for the effect. In the AgI-Ag_2O-V_2O_5 system, the increase depended on the interfacial area between glass and crystalline $Ag_8I_4V_2O_7$ inclusions. An interface related effect was also responsible for the conductivity enhancement in partially crystallized AgI-Ag_2O-P_2O_5 glasses. The absence of conductivity enhancement in the AgI-Ag_2O-B_2O_3 system was explained by formation of α-AgI microcrystals. When the conductivity of the crystallites is higher than that of the glassy matrix, the interface region is short-circuited. Ionic conduction follows comparable pathways in crystalline and glassy states.

One objective of the polymer composites development, which started at the end of the 1980s, is to improve the elastic and tensile properties of glasses and ceramics, which are often too hard and brittle to be useful as solid electrolytes. Skaarup et al. [106] first made polymer-ceramic composites using a large percentage of Li_3N in doped polyethylene-oxide (PEO) and insulating polyethylene matrices. Surprisingly, the latter were more conducting than the PEO composites, indicating that the polymer mainly holds the ceramic particles together, but does not provide an ionic conduction pathway. On the other hand, the ionic conductivity is often enhanced in amorphous polymer electrolytes, which behave as ''soft solids'' at the temperatures of operation. Croce et al. [107] added β''-alumina or $LiAlO_2$ to PEO electrolytes in order to improve the mechanical properties of the polymer.

Mixtures of NASICON with doped PEO showed smaller dc conductivity than either the pure ceramic or the pure polymer electrolyte. The considerably enhanced interface resistance was probably due to a poor contact between the two phases [108]. Two-phase mixtures of a Li-ion conducting $Li_{1+x}Al_xTi_{2-x}(PO_4)_3$ ceramic with an amorphous copolymer ethylene oxide-propylene oxide (3PEG) showed conductivities approaching bulk ceramic values, but the importance of pores was confirmed [109]. Tortet et al. investigated and modeled proton-conducting composites of an inert polymer (PPS) and brushite ($CaHPO_4$ 2 H_2O) [110].

Preparation problems, notably poor adhesion, pores and gaps at the phase boundaries, make the investigation of space charge effects in these materials difficult. In principle, modifications of local defect distribution are expected near any type of interface, but they are more or less important, depending on the chemical affinity between the two phases. Recently, Croce et al. [111] succeeded to prepare a polymer composite with dispersed TiO_2 nanoparticles with a significantly enhanced conductivity. This underlines that more preparative and theoretical efforts are needed to better

understand and further improve the properties of polymer-ceramic composites.

3.7. Ionic Conductor/Noble Metal Composites

Oxygen-permeable ceramic membranes are used for e.g., separation of oxygen from air. They are made from mixed conducting oxides, in which ambipolar diffusion of ionic and electronic charge carriers in an oxygen potential gradient assures a high oxygen permeation flux through the membrane. However, they suffer degradation with time due to either oxygen-ordering or compositional alteration under reducing conditions. Mixed oxide-ion and electronic conductivity is also observed in composites of a solid oxide-ion electrolyte and a noble metal, if percolating pathways exist for each component. These mixed-conducting oxide ceramic-metal composites (CERMETs), including Y-stabilized ZrO_2 with Pd [112], Sm-doped CeO_2 with Pd [113], rare-earth doped Bi_2O_3 with Ag [114], have an appreciable oxygen permeation rate at elevated temperature without degradation and are considered more attractive for industrial applications, although they are relatively expensive.

4. Conclusions and Future Trends

Interfaces allow a variety of optimization strategies for materials. Boundary effects on transport phenomena are of outstanding importance in ionic conductor composites: given their anisotropy, interfaces can act as transport pathways or transport barriers (core effect) and they can affect the charge carrier distribution in adjacent regions, due to defect segregation at the interface (space charge effect). Given the reduced interface core area in conventional ceramics and composites, the space charge effect is often more important for practical properties.

The conductivity enhancement observed in ceramic composite materials can be at least qualitatively understood and in some cases even quantitatively described by simple analytical equations derived from space charge theory. Many other experimental observations are also consistent with the ''abrupt core-space charge model''. However, more complicated situations can be encountered, for example when structural perturbations near interfaces extent over a larger range, including presence of dislocations or metastable phases. Space charge effects at interfaces between nanocrystalline inclusions and a glass matrix can also explain the conductivity enhancement in some glass-ceramic composites. In polymer-ceramic composites, the conductivity variations observed seem to be essentially related to macroscopic inter-particle voids, but recent work revealed the possibility of space charge effects.

To close, let us mention some future trends and research needs. Much remains to be done concerning fundamental properties of interfaces in composites, such as segregation and diffusion processes at phase boundaries. Other important issues related to composite materials, that have not been sufficiently investigated, are heterogeneous catalysis, the role of segregation and space charge effects in solid state reactions and sintering, and also in solid state photoelectrochemical devices. The spectacular improvement of inexpensive micro-computers over the last decade makes numerical computation of materials properties a lot easier. Besides the simulation of the electrical properties, such as the percolation approach mentioned in this article, one can predict substantial advances in the computer assisted design of composites with tailored properties in the next years.

Spectacular improvements of existing properties can be foreseen in composites with very small grains (nanocomposites), given that space charge theory predicts a supplementary increase in conductivity due to overlapping space charge regions, which leads to a more or less completely disordered ''bulk'' structure. Alternative methods to prepare nanocomposites, including thin-film techniques or partial crystallization of ion conducting glasses, should be developed. Given the relatively small number of investigations performed so far, the progress of polymer composites will certainly speed up in the next years. Apart from the need for solid electrolytes with suitable mechanical properties, ionic conductivity may be improved by better knowledge of the interface properties, including studies of the possibility of space charge effects in the ceramic-polymer boundary region in dense composites.

Acknowledgment

The author apologizes to all colleagues, whose contribution to the topic of this review may have

been overlooked by mistake or not adequately appreciated. The bibliographic help by H. Desvals is greatly appreciated. J.-M. Debierre and Y. Massiani are gratefully acknowledged for a careful reading of the manuscript.

References

1. F.A. Kröger, *The Chemistry of Imperfect Solids* 2nd edition (North-Holland, Amsterdam, 1974).
2. J. Maier, *Prog. Solid St. Chem.*, **23**, 171 (1995).
3. C.C. Liang, *J. Electrochem. Soc.*, **120**, 1289 (1973).
4. J.B. Wagner, in *High Conductivity Solid Ionic Conductors* T. Takahashi, ed. (World Scientific, Singapore, 1989).
5. G. Gouy, *J. Chim. Phys.*, **29**, 145 (1903).
6. J.W. Verwey and J.Th.G. Overbeek, *Theory of the Stability of Lyophobic Colloids* (Elsevier, New York, 1948).
7. K. Lehovec, *J. Chem. Phys.*, **21**, 1123 (1953).
8. C. Wagner, *J. Phys. Chem. Solids*, **33**, 1051 (1972).
9. T. Jow and J.B. Wagner, *J. Electrochem. Soc.*, **126**, 1963 (1979).
10. J. Maier, *J. Phys. Chem. Solids*, **46**, 309 (1985).
11. J. Maier, *J. Electrochem. Soc.*, **134**, 1524 (1987).
12. R.C. Agrawal and R.K. Gupta, *J. Mater. Sci.*, **34**, 1131 (1999).
13. A. Atkinson, *Solid State Ionics*, **28–30**, 1377 (1988).
14. B.J. Wuensch and H.L. Tuller, *J. Phys. Chem. Sol.*, **55**, 975 (1994).
15. M. Aoki, Y.-M. Chiang, I. Kosacki, J.-R. Lee, H.L. Tuller, and Y. Liu, *J. Am. Ceram. Soc.*, **79**, 1169 (1996).
16. J.A.S. Ikeda and Y.-M. Chiang, *J. Am. Ceram. Soc.*, **76**, 2437 and 2447 (1993).
17. D.A. Blom and Y.-M. Chiang, *Mat. Res. Soc. Symp. Proc.*, **458**, p. 127 (Materials Research Society, 1997).
18. K. Shahi and J.B. Wagner, *Solid State Ionics*, **3/4**, 295 (1981).
19. U. Lauer and J. Maier, *Ber. Bunsenges. Phys. Chem.*, **96**, 111 (1992).
20. U. Lauer and J. Maier, *Solid State Ionics*, **51**, 209 (1992).
21. S. Gupka, S. Patnaik, and K. Shahi, *Solid State Ionics*, **31**, 5 (1988).
22. J. Maier, *Solid State Ionics*, **23**, 59 (1987).
23. J. Maier, *Phys. Stat. Sol. (a)*, **112**, 115 (1989).
24. J. Maier, S. Prill, and B. Reichert, *Solid State Ionics*, **28–30**, 1465 (1988).
25. J. Maier, *Solid State Ionics*, **18/19**, 1141 (1986).
26. N.J. Dudney, *J. Amer. Ceram. Soc.*, **70**, 65 (1987).
27. D. Lubben and F.A. Modine, *J. Appl. Phys.*, **80**, 5150 (1996).
28. J.B. Phipps and D.H. Whitmore, *Solid State Ionics*, **9/10**, 123 (1983).
29. S. Jiang and J.B. Wagner, *J. Phys. Chem. Solids*, **56**, 1101 (1995).
30. J.-S. Lee, St. Adams, and J. Maier, *Solid State Ionics*, in press.
31. J. Maier and B. Reichert, *Ber. Bunsenges. Phys. Chem.*, **90**, 666 (1986).
32. J. Maier, *Ber. Bunsenges. Phys. Chem.*, **88**, 1057 (1984).
33. M. Nagai and T. Nishino, *Solid State Ionics*, **117**, 317 (1999).
34. G. Simkovich and C. Wagner, *J. Catalysis*, **1**, 521 (1962).
35. P. Murugaraj and J. Maier, *Solid State Ionics*, **32/33**, 993 (1989).
36. N. Aoyama, Y. Yamashita, A. Abe, and N. Takezawa, *Phys. Chem. Chem. Phys.*, **1**, 3365 (1999).
37. M. Vennekamp and J. Janek, *Solid State Ionics*, **118**, 43 (1999).
38. A.M. Stoneham, E. Wade, and J.A. Kilner, *Mater. Res. Bull.*, **14**, 661 (1979).
39. J.C. Wang and N.J. Dudney, *Solid State Ionics*, **18/19**, 112 (1986).
40. N.F. Uvarov, V.P. Isupov, V. Sharma, and A.K. Shukla, *Solid State Ionics*, **51**, 41 (1992).
41. A.K. Bhattacharyya, T.R. Middya, and S. Tarafdar, *Ionics*, **2**, 346 (1996).
42. B. Nettelblad, B. Zhu, and B.-E. Mellander, *Phys. Rev. B*, **55**, 6232 (1997).
43. A. Bunde, W. Dieterich, and H.E. Roman, *Phys. Rev. B*, **34**, 3439 (1986).
44. A. Bunde, W. Dieterich, and H.E. Roman, *Solid State Ionics*, **18/19**, 147 (1986).
45. A. Bunde, *Solid State Ionics*, **28–30**, 34 (1988).
46. H.E. Roman and M. Yussouf, *Phys. Rev. B*, **36**, 7285 (1987).
47. C. DeW. Van Siclen, *Phys. Rev. E*, **59**, 2804 (1999).
48. J.-M. Debierre, P. Knauth, and G. Albinet, *Appl. Phys. Lett.*, **71**, 1335–1337 (1997).
49. P. Knauth, G. Albinet, and J.-M. Debierre, *Solid State Ionics*, **121**, 101 (1999).
50. C. Lambert, L. Memoli, J.-M. Debierre, P. Knauth, and G. Albinet, *Ionics*, **5**, 200 (1999).
51. L. Tortet, J.-R. Gavarri, J. Musso, G. Nihoul, J.-P. Clerc, A.N. Lagarkov, and A.K. Sarychev, *Phys. Rev. B*, **58**, 5390 (1998).
52. R. Blender and W. Dieterich, *Solid State Ionics*, **28–30**, 82 (1988).
53. M. Nagai and T. Nishino, *J. Electrochem. Soc.*, **138**, L49 (1991).
54. M. Nagai and T. Nishino, *Solid State Ionics*, **53–56**, 63 (1992).
55. M. Nagai and T. Nishino, *Key Engineering Materials*, **111–112**, 281 (1995).
56. M. Nagai and T. Nishino, *Solid State Ionics*, **79**, 319 (1995).
57. G. Rog, A. Kielski, A. Kozlowska-Rog, and M. Bucko, *Ceramics International*, **24**, 91 (1998).
58. J. Köhler, Y. Kobayashi, N. Imanaka, and G. Adachi, *Solid State Ionics*, **113–115**, 553 (1998).
59. Y. Saito, K. Hariharan, and J. Maier, *Solid State Phenomena*, **39–40**, 235 (1994).
60. K. Hariharan and J. Maier, *J. Electrochem. Soc.*, **142**, 3469 (1995).
61. B. Zhu, Z.H. Lai, and B.-E. Mellander, *Solid State Ionics*, **70/71**, 125 (1994).
62. A. Kumar and K. Shahi, *Mater. Res. Bull.*, **31**, 877 (1996).
63. M. Tatsumisago, T. Saito, and T. Minami, *Solid State Ionics*, **70/71**, 394 (1994).
64. St. Adams, K. Hariharan, and J. Maier, *Solid State Ionics*, **86–88**, 503 (1996).
65. U. Lauer and J. Maier, *J. Electrochem. Soc.*, **139**, 1472 (1992).
66. G. Ardel, D. Golodnitsky, E. Peled, Y. Wang, G. Wang, S. Bajue, and S. Greenbaum, *Solid State Ionics*, **113–115**, 477 (1998).
67. A. Lunden, B.-E. Mellander, A. Bengtzelius, H. Ljungmark, and R. Tärneberg, *Solid State Ionics*, **18/19**, 514 (1986).

68. A.C. Khandkar and J.B. Wagner, *Solid State Ionics*, **18/19**, 1100 (1986).
69. A. Khandkar, V.B. Tare, A. Navrotsky, and J.B. Wagner, *J. Electrochem. Soc*., **131**, 2683 (1984).
70. J. Rogez, A. Garnier, and P. Knauth, *J. Phys. Chem. Solids*, in press.
71. S. Pack, B. Owens, and J.B. Wagner, *J. Electrochem. Soc*., **127**, 2177 (1980).
72. F.W. Poulsen, N.H. Anderson, B. Kindl, and J. Schoonman, *Solid State Ionics*, **9–10**, 119 (1983).
73. O. Yamamoto, in *Solid State Electrochemistry* P.G. Bruce, ed. (Cambridge University Press, 1995).
74. B.C. Tofield and D.E. Williams, *Solid State Ionics*, **9/10**, 1299 (1983).
75. B. Zhu, Z.H. Lai, and B.-E. Mellander, *Solid State Ionics*, **70/71**, 125 (1994).
76. M.A.K.L. Dissanayake and B.-E. Mellander, *Solid State Ionics*, **21**, 279 (1986).
77. K. Singh and S.S. Bhoga, *Solid State Ionics*, **40/41**, 1025 (1990).
78. Q.G. Liu and W.L. Worrell, *Solid State Ionics*, **18/19**, 524 (1986).
79. M.M.E. Jacob, S. Rajendran, R. Gangadharan, M.S. Michael, and S.R.S. Prabaharan, *Solid State Ionics*, **86–88**, 595 (1996).
80. M. Nagai and T. Nishino, *Solid State Ionics*, **70/71**, 96 (1994).
81. U. Guth, S. Brosda, B. Löscher, A. Simmich, P. Schmidt, and H.-H. Möbius, *Mater. Sci. Forum*, **76**, 137 (1991).
82. S. Brosda, H.J.M. Bouwmeester, and U. Guth, *Ionics*, **2**, 323 (1996).
83. Y. Saito, J. Mayne, K. Ado, Y. Yamamoto, and O. Nakamura, *Solid State Ionics*, **40/41**, 72 (1990).
84. T. Takeuchi, K. Ado, Y. Saito, M. Tabuchi, C. Masquelier, and O. Nakamura, *Solid State Ionics*, **79**, 325 (1995).
85. T. Takeuchi, K. Ado, Y. Saito, M. Tabuchi, H. Kageyama, and O. Nakamura, *Solid State Ionics*, **89**, 345 (1996).
86. T. Takeuchi, K. Ado, Y. Saito, M. Tabuchi, H. Kageyama, and O. Nakamura, *Solid State Ionics*, **86–88**, 565 (1996).
87. G.V. Lavrova, V.G. Ponomareva, and N.F. Uvarov, *Solid State Ionics*, in press.
88. N.F. Uvarov, P. Vanek, Yu.I. Yuzyuk, V. Zelezny, V. Studnicka, B.B. Bokhonov, V.E. Dulepov, and J. Petzelt, *Solid State Ionics*, **90**, 201 (1996).
89. J. Maier, *Solid State Ionics*, **86–88**, 55 (1996).
90. K. Shahi and J.B. Wagner, *J. Electrochem. Soc*., **128**, 6 (1981).
91. N.F. Uvarov, E.F. Hairetdinov, B.B. Bokhonov, and N.B. Bratel, *Solid State Ionics*, **86–88**, 573 (1996).
92. M. Nagai and T. Nishino, *J. Am. Ceram. Soc*., **76**, 1057 (1993).
93. R.C. Agrawal, M.L. Verma, and R.K. Gupta, *J. Phys. D*, **31**, 2854 (1998).
94. A. Chandra, A. Spangenberg, and J. Maier, *J. Electroceramics*, **3**, 45 (1999).
95. K. Tennakone, G.R.R.A. Kumara, I.R.M. Kottegoda, K.G.U. Wijayantha, and V.P.S. Perera, *J. Phys. D : Appl. Phys*., **31**, 1492 (1998).
96. M.-A. Desvals and P. Knauth, *J. Phys. Chem. Solids*, **58**, 319–325 (1997).
97. A. Becquart, F. Cabané, and P. Knauth, *J. Electroceramics*, **1**, 173–177 (1997).
98. P. Knauth, G. Albinet, and J.-M. Debierre, *Ber. Bunsenges. Phys. Chem*., **102**, 945–952 (1998).
99. S. Fujitsu, K. Koumoto, and H. Yanagida, *Solid State Ionics*, **18/19**, 1146 (1986).
100. S.L. Finch and R.V. Kumar, *Proc. 6th Euroconference on Solid State Ionics* (1999) p. 59.
101. J. Köhler, N. Imanaka, and G. Adachi, *Solid State Ionics*, **122**, 173 (1999).
102. M. Nagai, K. Ogawa, and T. Nishino, *J. Am. Ceram. Soc*., **77**, 2470 (1994).
103. A.J. Feighery and J.T.S. Irvine, *Solid State Ionics*, **121**, 209 (1999).
104. M. Mori, T. Abe, and H. Itoh, *Solid State Ionics*, **74**, 157 (1994).
105. M. Tatsumisago, Y. Shinkuma, and T. Minami, *Nature*, **354**, 217 (1991).
106. S. Skaarup, K. West, P.M. Julian, and D.M. Thomas, *Solid State Ionics*, **40/41**, 1021 (1990).
107. F. Croce, S. Passerini, A. Selvaggi, and B. Scrosati, *Solid State Ionics*, **40/41**, 375 (1990).
108. J. Plocharski and W. Wieczorek, *Solid State Ionics*, **28–30**, 979 (1988).
109. K.M. Nairn, A.S. Best, P.J. Newman, D.R. MacFarlane, and M. Forsyth, *Solid State Ionics*, **121**, 115 (1999).
110. L. Tortet, J.-R. Gavarri, J. Musso, G. Nihoul, and A.K. Sarychev, *J. Solid State Chem*., **141**, 392 (1998).
111. F. Croce, G.B. Appetecchi, L. Persi, and B. Scrosati, *Nature*, **394**, 456 (1998).
112. T.J. Mazanec, *Solid State Ionics*, **70/71**, 11 (1994).
113. K. Huang, M. Schroeder, and J.B. Goodenough, *Electrochem. Solid State Lett*., **2**, 375 (1999).
114. J.E. ten Elshof, N.Q. Nguyen, M.W. den Otter, and H.J.M. Bouwmeester, *J. Electrochem. Soc*., **144**, 4361 (1997).